applied sciences

MDPI

Communication

Superconducting Electronic–Photonic Platform for HEB-Based Terahertz Spectrometers

Alexander Shurakov [1,2,*], Ivan Belikov [1,2], Anatoliy Prikhodko [1,2], Margarita Ershova [1] and Gregory Goltsman [1,2]

[1] Department of General and Experimental Physics, Moscow Pedagogical State University, 1/1 Malaya Pirogovskaya St., Moscow 119991, Russia
[2] Tikhonov Moscow Institute of Electronics and Mathematics, National Research University Higher School of Economics, 20 Myasnitskaya St., Moscow 101000, Russia
* Correspondence: alexander@rplab.ru

Abstract: Terahertz photonic integrated circuits are becoming popular in ultrafast on-chip signal generation and processing. They outperform assemblies of electronic devices making use of metallic waveguides in term of both fabrication complexity and system losses. In this study, we report on a nearly all-dielectric hot electron bolometer mixer compatible with the technology of integrated Si photonic crystals. The developed on-chip power distribution networks ensure input losses of 2.4 dB and far-field radiation patterns with a gain of 12.1 dB and a side lobe level below −11 dB. The mixer is designed for spectral measurements at 2.7 THz. It can be used either as a part of an on-chip spectrometer or as a standalone device.

Keywords: terahertz; hot electron bolometer; frequency mixer; silicon-on-insulator; photonic crystal; photonic-integrated circuit

check for updates

Citation: Shurakov, A.; Belikov, I.; Prikhodko, A.; Ershova, M.; Goltsman, G. Superconducting Electronic–Photonic Platform for HEB-Based Terahertz Spectrometers. *Appl. Sci.* **2023**, *13*, 5892. https://doi.org/10.3390/app13105892

Academic Editors: Vladimir L. Vaks, Valery P. Koshelets and Alexei N. Baranov

Received: 21 March 2023
Revised: 24 April 2023
Accepted: 4 May 2023
Published: 10 May 2023

1. Introduction

Over the past few decades, the terahertz (THz) frequency band has attracted the attention of the scientific community in a variety of applications. The unique properties of THz radiation to harmlessly penetrate through non-metallic objects and biological tissues are useful for imaging and spectral measurements in medical and security systems, materials science and so forth [1–4].

Number of recent studies suggests that THz photonic integrated circuits (PICs) are worth using in the next-generation wireless communications for an ultrafast on-chip THz signal generation and processing [5,6]. Above 300 GHz, they mostly rely on a silicon platform and make use of either a topological or photonic crystal waveguides. Silicon PICs enable creation of THz circuits with numerous passive and active components interacting through low-loss dielectric media. They are especially in demand at frequencies beyond 1 THz, where performance of planar metallic waveguides conventionally used in THz electronic circuits is compromised [7,8]. Use of photonic power distribution networks (PPDNs) not only enable reduction of on-chip propagation losses, but aids to avoid numerous issues related to packaging and assembly. With the appearance of modern solutions in THz PPDNs [9], flexibility in designing PIC grows. Synergy of electronic and photonic handling of THz signals is recognized as one of the most promising options [10]. However, development of non-linear frequency conversion devices naturally compatible with silicon PIC platform is at an early stage. In this study, we propose design of a THz hot electron bolometer (HEB) mixer that comprises a silicon photonic crystal waveguide integrated with two dielectric rod antenna (DRA) arrays through multimode interference power combiners. These arrays are to couple an HEB element with local oscillator (LO) and signal at 2.7 THz. The proposed design is based on low-loss conversion of a THz wave propagating in dielectric media into currents inside an HEB element. In contrast to the recently reported HEB-based PIC for classical and quantum photonics at telecommunication wavelengths [11], our study addresses the issue of coupling efficiency between a dielectric waveguide and a superconducting microbridge much smaller than the guided wave.

Superconducting HEB mixers are well known for their decent performance in the THz frequency band above 1 THz. They are traditionally in demand by radio astronomy for THz spectral line measurements, when superconductor-insulator-superconductor (SIS) and Schottky diode mixers face their fundamental limits and technological barriers [12,13]. An HEB mixer requires extremely low LO power as compared to the semiconductor competitors. Furthermore, it is intrinsically a frequency non-selective electronic device, whose spectral features are predefined by the input optics design [14]. Modern THz HEB-based spectrometers rely on both quasioptical and waveguide designs of the mixers. Their operating bands are determined by the scientific interest to spectral signatures for different phases of the interstellar medium (ISM). The ISM phase tracers of interest are presented by [CII] at 1.9 THz, [HD] at 2.7 THz, [NII] at 2.45 and 5.23 THz, [OI] at 2.1 and 4.7 THz, and [OIII] at 3.4 and 5.8 THz [15]. Heterodyne HEB-aided observations at 4.7 THz are the focus of several upcoming balloon and space missions [16,17]. Atmospheric transmittance of beyond 40% in number of windows within 7–14 THz enables ground-based observations in Antarctica [18]. This provides a good opportunity for studies of exoplanet formation and energy balance in ISM. At these frequencies, however, fabrication and packaging of electronic devices become technologically challenging. There are no examples of spectral instruments for radio astronomy operated beyond 7 THz so far. We believe that use of a superconducting electronic–photonic platform can simplify implementation of an HEB-based spectrometer for 7–14 THz operation. In addition, it can significantly increase flexibility in integrating components of the spectrometer front-end.

2. Materials and Methods

In this section, we focus on the input optics of an HEB mixer utilizing Si waveguiding structures. The basic concept and expected performance of the mixer are further discussed in terms of both electromagnetic (EM) modeling and prototyping of its key structural elements.

Transfer of an EM field energy from one point of space to another is one of the most fundamental tasks in number of practical applications. The transfer can be maintained via transmission lines or with the aid of free space optics relying on the use of transmitting and receiving antennas. The choice of antenna type is determined by the demands of a specific application and has to be compliant with requirements on its beam pattern and matching with a feeding network. In turn, these parameters can be noticeably tuned for a given type of antenna if a phased antenna array is implemented [19].

Upon use of PPDNs, two general options are available for coupling PIC with external signal sources. The first option is to use a grating coupler and to receive signal along the axis perpendicular to the PIC plane. Such a technique is capable of providing input losses as low as 1 dB over a fractional bandwidth of 3–5% [20]. The second option is related to end-fire coupling. This technique relies on the injection of external Gasussian beam into the unloaded end of a dielectric waveguide terminating PIC. The injection is maintained along the waveguide axis either directly or through a mode size transformer [21]. This devise is basically a dielectric taper. It can be effectively used in either a directive reception/transmission of EM radiation from/into a free space or in maintaining transition from hollow metallic waveguides to PPDNs and vice versa. In our design, we choose an end-fire coupling as a proof-of-concept solution. It ensures implementation simplicity at the stage of cleanroom fabrication and, later on, during packaging and assembly at the final stage. We develop a dielectric taper structure acting as DRA [22,23] in a four-element linear antenna array operated at 2.7 THz. The array output is harvested by a 4×1 ports multimode interference power combiner (MMIPC), which is terminated by a photonic crystal waveguide (PCWG). The latter, in turn, is integrated with an HEB-loaded tapered slot line (TSL). The coupling scheme is used for the implementation of signal and LO input lines of a nearly all-dielectric mixer.

Figure 1 provides a three-dimensional (3D) model of a nearly all-dielectric HEB mixer designed for operation at 2.7 THz. Openings in Si are used to define geometries of MMIPC and PCWG. Four-wire biasing of the HEB element is implemented.

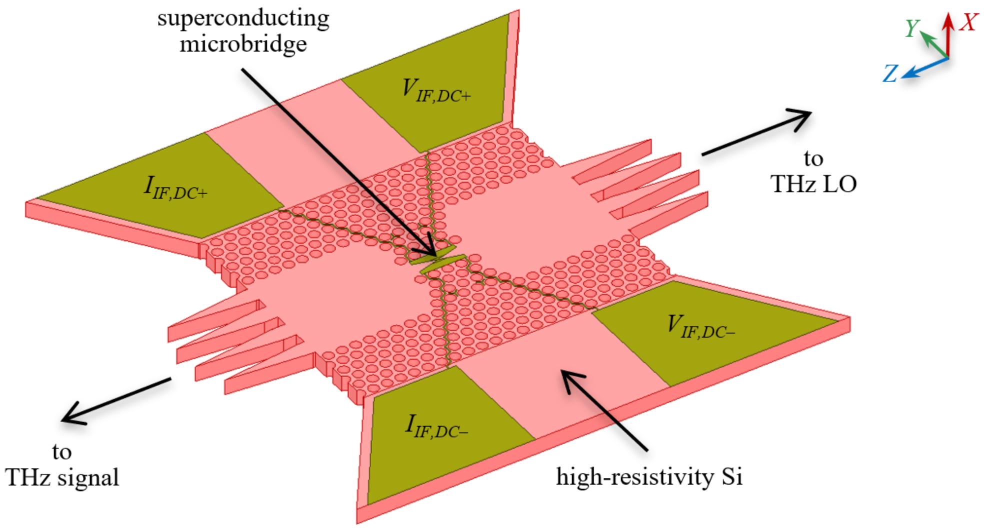

Figure 1. A 3D model of a nearly all-dielectric THz HEB mixer.

The conversion of an EM wave propagating in dielectric media into an alternating current (AC) inside HEB is the core in the proposed design. The conversion can be maintained by coupling HEB to PCWG either directly or through a planar metallic probe. There are examples of the former implementation in infrared (IR) range [11]. At 2.7 THz, however, the working area of the superconducting film is expected to be quite large, since the wavelength of EM radiation in Si equals 32 µm. This consequently leads to a drastic increase in the LO power required for operation of the mixer. Potential use of plasmonic antennas for enhanced coupling faces the same issue [24]. Alternatively, when TSL is employed as an EM probe, conventional linear dimensions of the superconducting film not exceeding a few microns can be chosen.

3. Results and Discussion

In this section, we provide details on a superconducting electronic–photonic platform suitable for the implementation of a 2.7 THz HEB mixer. Developed THz components are evaluated by prototyping at enlarged and actual scales. The evaluation includes (a) beam pattern measurements of THz signal and LO input lines at 51 GHz and (b) analysis of the superconducting properties of a full-size HEB mixer. We also evaluate fabrication tolerances for cleanroom processes and discuss perspectives.

3.1. EM Simulations

Figure 2 illustrates effective transition from a single-mode Si ribbon waveguide to a 50 Ω microbridge developed via EM simulations. We use HFSS 15 as simulation software. Dielectric losses in Si are neglected, and its relative permittivity is set to 11.9. The waveguide side walls are surrounded by quarter-wave vacuum insets terminated by radiation boundaries. Front and rear ends of the waveguide are excited by two wave ports (ports 1 and 2). We can control coupling between the ports with the aid of a distributed Bragg reflector (DBR). The reflector is presented by a triplet of openings with diameters D_1, D_2, D_3 in the waveguide at the THz signal input. The HEB-loaded tapered slot line is modeled as a golden sheet with a lumped port implemented in the center (port 3). Geometric parameters of the transition developed for 2.7 THz operation are detailed in Table 1.

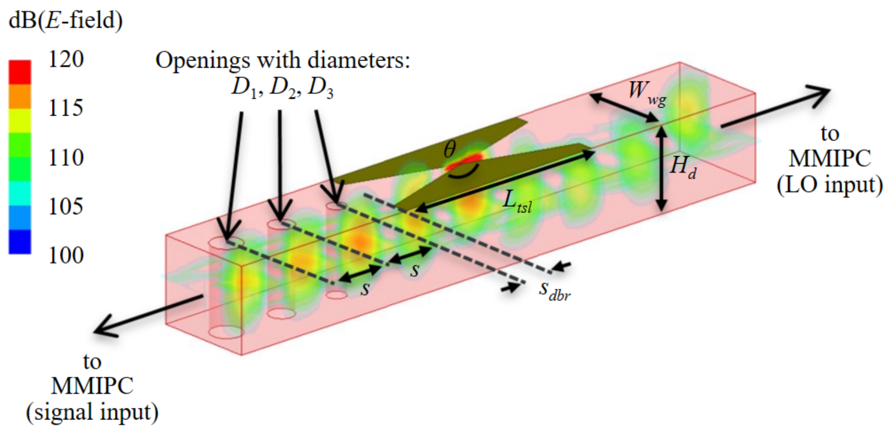

Figure 2. EM model of a 2.7 THz Si ribbon waveguide integrated with a 50 Ω-loaded TSL.

Table 1. Geometry of a 2.7 THz Si ribbon waveguide integrated with a 50 Ω-loaded TSL.

H_d [µm]	W_{wg} [µm]	L_{tsl} [µm]	θ [°]	s_{dbr} [µm]	s [µm]	D_1 [µm]	D_2 [µm]	D_3 [µm]
27	32	70.9	146	11.9	21	10	8	6

We observe reflection and transmission coefficients with magnitudes $S33 = -16.1$ dB and $S31 = S32 = -4.4$ dB for a DBR free transition. In the presence of DBR, $S33 = -32.3$ dB, $S31 = -2.4$ dB, and $S32 = -7.1$ dB. A further increase of $S31$ up to approximately -1 dB is possible at the expense of a drastic decrease of $S32$. This option becomes attractive, for instance, if one designs an incoherent detector and LO is not required. For the transition from a ribbon waveguide to PCWG, the coupling efficiency can also be increased by a two-step-size tapered photonic crystal structure with a defect opening in the center [25].

To improve efficiency of an end-fire coupling, front and rear waveguide ends of the developed transition are terminated by Si forked antennas. Each antenna is presented by a four-element DRA array integrated with 4 × 1 ports MMIPC, as depicted in Figure 3.

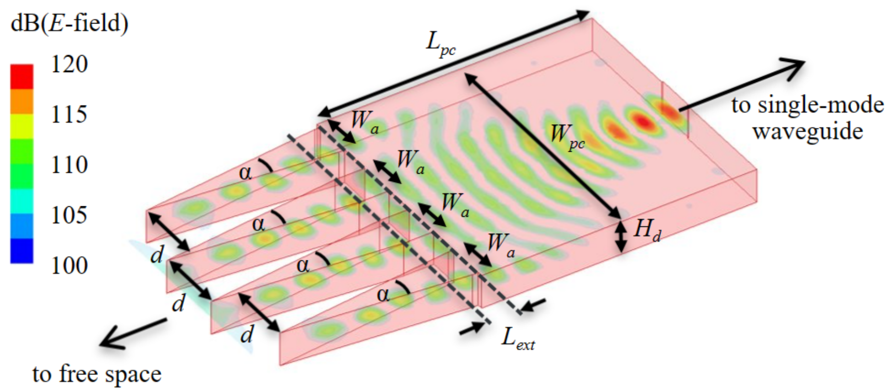

Figure 3. EM model of a 2.7 THz Si DRA array integrated with MMIPC.

The MMIPC design relies on the use of an Si ribbon waveguide supporting propagation of multiple lateral modes. Such a condition is achieved for effective width of the waveguide defined as [26]:

$$W_{eff} = \frac{\pi(m+1)}{k_{ym}}, \tag{1}$$

where m is the mode number and k_{ym} is the lateral wavenumber of the m-th mode. Due to a blur of the interface between the dielectric medium and vacuum, the actual width of the waveguide, W_{pc}, becomes smaller. Its deviation from W_{eff} is defined by Equation (2):

$$W_{pc} = W_{eff} - \frac{\lambda_0}{\pi \epsilon_r^{\sigma} \sqrt{\epsilon_r - 1}}, \tag{2}$$

where λ_0 is the free space wavelength, ϵ_r is the relative permittivity of a dielectric medium, and σ is the constant factor equal to 0 for transverse electric and 1 for transverse magnetic modes. The length of the waveguide, L_{pc}, usually obeys Equation (3); however, it may experience a reduction of 17–23% in case of compact devices made of low-permittivity dielectrics [27]:

$$L_{pc} = \frac{W_{eff}^2 \sqrt{\epsilon_r}}{4\lambda_0}. \tag{3}$$

Harvesting of each supported m-th mode at the output of the DRA array is maintained by MMIPC with a corresponding phase constant, defined as:

$$\beta_m = \frac{2\pi\sqrt{\epsilon_r}}{\lambda_0} - \frac{\pi\lambda_0 (m+1)^2}{4W_{eff}^2 \sqrt{\epsilon_r}}. \tag{4}$$

Superposition of the harvested modes results in four equally spaced power maxima at the MMIPC input. Almost 90° phase delays appear in the lateral ports of the combiner with respect to the central ones. To implement a uniform linear array with a zero-phase increment between antennas, we extend two central DRAs by Si ribbon inserts. Details on the geometry developed for the 2.7 THz operation are summarized in Table 2. This geometry ensures simulated gain of 12 dB with a corresponding side lobe level of −13.1 dB and decent matching to a single-mode Si waveguide. The half-power beamwidth equals 26° in the DRA array plane. In the EM simulations, as before, dielectric losses in Si are neglected, and its relative permittivity is set to 11.9. When calculating the radiation pattern of the DRA array integrated with MMIPC, we rely on the principle of reversibility and simulate its performance in a transmitting mode. The MMIPC side walls and the DRA array are surrounded by quarter-wave vacuum insets terminated by radiation boundaries. The MMIPC single output is excited by a wave port. The port has linear dimensions of $0.648\lambda_0 \times 0.324\lambda_0$ (width × height), mode polarity is set using integration lines, and no post processing is performed.

Table 2. Geometry of a 2.7 THz Si DRA array integrated with MMIPC.

H_d [µm]	W_{pc} [µm]	L_{pc} [µm]	W_a [µm]	L_{ext} [µm]	α [°]	d [µm]
27	205.6	222.2	30.6	19.5	12	55.5

Footprints of the developed Si antennas and the transition from a Si ribbon waveguide to a 50 Ω microbridge are further used in the design of a nearly all-dielectric HEB mixer. Referring to Figure 4, we use the technology of integrated Si photonic crystals to define contours of the mixer structural elements. Hexagonal lattice of openings with a diameter $D = 18$ µm and lattice constants $A_Z = 23.4$ µm, $A_Y = 40.5$ µm is implemented in a 27 µm thick Si substrate. Driven by the lattice constraints, we choose $W_{pc} = 194.1$ µm and $L_{pc} = 213.2$ µm. The distances are measured between tangents to the inner edges of openings defining contour of MMIPC. Spacing between DRAs $d = 50.9$ µm. Other geometric parameters remain unchanged.

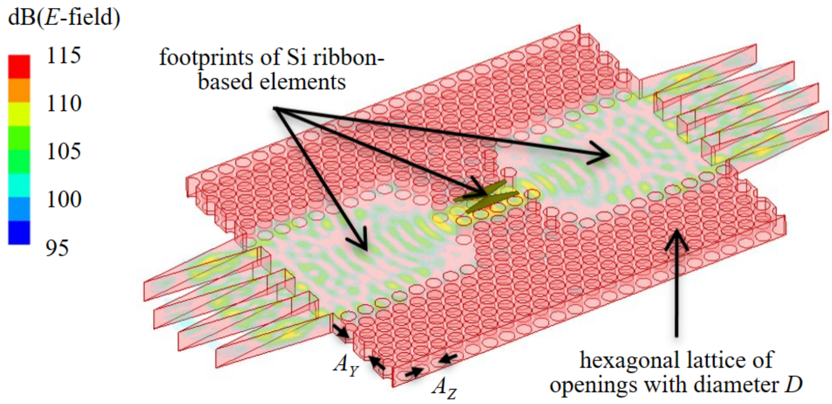

Figure 4. EM model of a nearly all-dielectric 2.7 THz HEB mixer based on integrated Si photonic crystals.

Analysis of the EM field pattern in the developed PIC reveals no degradation of the mixer input losses upon integration of its elements. Radiation patterns of THz input lines, however, are affected by the changes in geometry of MMIPCs and boundary conditions at their laterals and outputs. Thus, revised Si forked antennas demonstrate gain of 12.1 dB with a side lobe level of −11 dB. The half-power beamwidth equals 17° in the PIC plane. Given that the integrated Si waveguiding structure makes use of photonic crystals and multimode interference effects, its operation frequency band is narrow. However, it covers at least three times the intermediate frequency bandwidth of a typical HEB mixer which is sufficient from a practical point of view. Furthermore, the achievable input losses of 2.4 dB compete with those in the input optics of THz receivers making use of conventional hollow metallic waveguides at 2.7 THz and outperform them in the range of 7–14 THz [9].

To confirm and complete our findings, we perform prototyping of the developed Si structures at an enlarged scale.

3.2. Prototyping

We fabricate a 50:1 scale prototype of Si forked antenna via direct machining of a dielectric substrate with relative permittivity of 10.2 and loss tangent of 0.003. A computer-aided milling and drilling process with a resolution in tool positioning of 0.625 μm is employed. The fabricated prototype utilizes integrated photonic crystals with $D = 1$ mm, $A_Z = 1.26$ mm, and $A_Y = 2.18$ mm. The following geometric parameters are implemented: $H_d = 1.52$ mm, $W_{pc} = 10.46$ mm, $L_{pc} = 11.5$ mm, $W_a = 1.65$ mm, $L_{ext} = 1.05$ mm, $\alpha = 12°$, and $d = 3$ mm. The prototype is also equipped with a 10° lateral taper at its output for coupling with hollow metallic waveguides of the measurement equipment.

Referring to Figure 5, the experimental setup for beam profile measurements comprises a microwave frequency synthesizer, rotary stage, waveguide diode detector, and a lock-in amplifier. The synthesizer provides a 51 GHz continuous waveform (CW), with amplitude modulation (AM) at 1 kHz, widespread into a free space. The antenna prototype is coupled with a WR-15 input of the detector. The latter, in turn, is mounted on the rotary stage placed far behind a Frauhoffer distance in front of the synthesizer. The response voltage from the detector is fed into a lock-in amplifier. We use a microwave absorber to filter out spurious ambient radiation. For peak incident power levels of 0.28 μW, the detector response voltage equals 550 μV. Given that the detector noise voltage of 0.04 μV is measured, we can conclude that the detector is operated within its specified dynamic range of 44–45 dB during the measurements.

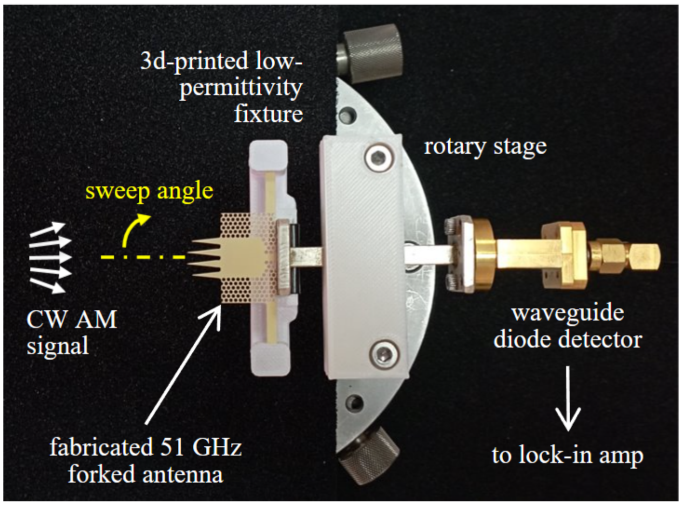

Figure 5. Experimental setup for beam profile measurements at 50–52 GHz.

As one can see in Figure 6, far-field beam of the fabricated 51 GHz forked antenna has a 27° wide main lobe with high Gaussisity in the antenna plane. The observed side lobe level does not exceed −12 dB, which outperforms similar low-permittivity designs earlier reported in the literature [27]. Experimental data are in good agreement with the results of EM simulations. The latter, in turn, predict the antenna gain of 11.2 dB with a side lobe level of −12.1 dB and a half-power beamwidth of 21° for the geometry developed. Such a behavior is also consistent with the forecasts of the 2.7 THz EM models for the Si platform. A further increase in the beam directivity is possible upon combining the developed dielectric forked antennas in linear or planar arrays.

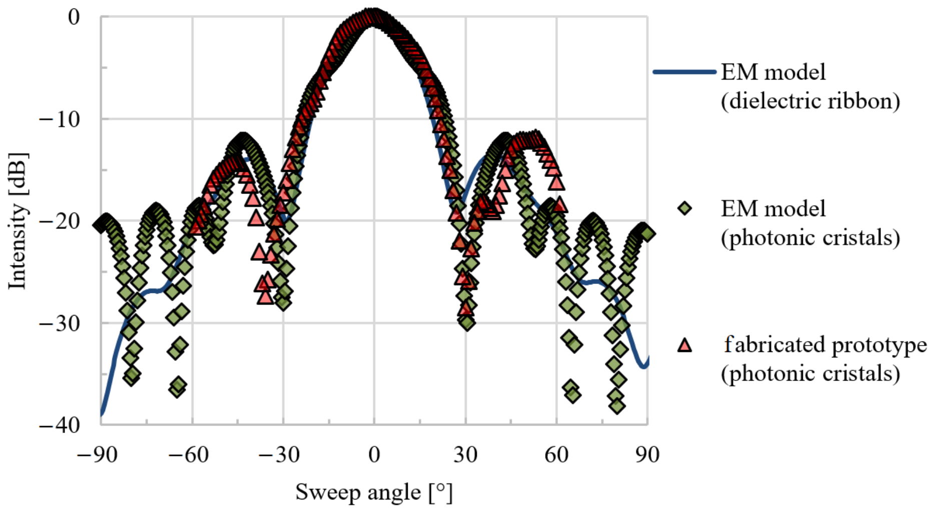

Figure 6. Beam profiles of dielectric forked antennas designed for operation at 50–52 GHz.

We also consider feasibility of prototyping for the entire PIC of an HEB mixer. A superconducting microbridge can be replaced by a microwave Schottky diode integrated with TSL. However, our machinery enables milling cuts only beyond 200 µm. It drastically exceeds linear dimensions of a scaled-up 50 Ω microbridge acting as an HEB element in EM simulations. This, in turn, largely affects coupling between elements of the PIC. However, specific propagation losses in dielectric waveguides with the chosen photonic crystal geometry of below 0.1 dB/mm were preliminary measured by us in [28]. This suggests that the ultimate sensitivity of the mixer is not compromised by input losses in the developed PPDNs.

3.3. Cleanroom Process

Driven by the results of EM simulations and prototyping, we choose a silicon-on-insulator (SOI) substrate with the following layered structure. The topmost layer is presented by a 27 µm thick high-resistivity Si. It is implemented on a 1 µm thick SiO_2 acting as an etch-stopper upon processing of the topmost layer and 300 µm thick Si handle-wafer.

The cleanroom fabrication process includes:

- Deposition and patterning of an NbN microbridge integrated with Ti/Au bias lines on the topmost layer of SOI substrate;
- Fabrication of a hexagonal lattice of openings in the topmost layer by the Bosch process;
- Rear-side removal of the Si handle-wafer and SiO_2.

A scanning electron microscope (SEM) image of the fabricated HEB mixer is provided in Figure 7. The mixer is based on a 4 nm thick NbN film, which has a critical temperature of 8.7 K with a transition width of 0.7 K and critical current density of 2.5 MA/cm^2. Sheet resistance of the film equals 830 Ω at room temperature. The sensitive element of the mixer is presented by an NbN bridge with nominal linear dimensions of 0.2 µm × 2.0 µm (length × width). We observe a mean value of room temperature resistance of 73 Ω for the mixers produced. This suggests that the bridge area slightly deviates due to imperfections in e-beam-assisted patterning of NbN film and Ti/Au contacts.

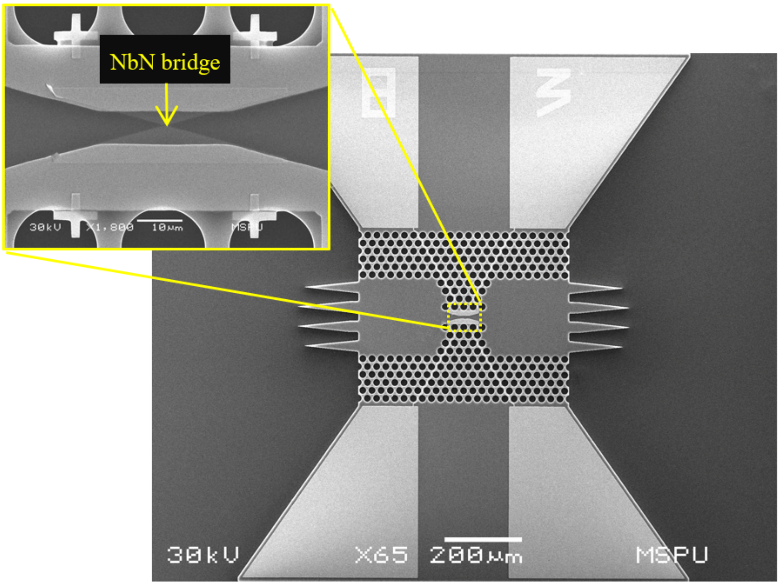

Figure 7. SEM image of a fabricated, nearly all-dielectric 2.7 THz HEB mixer.

For the implemented geometry of Si photonic crystals, we measure $D = 18.27 \pm 0.47$ µm. The mean value differs from the nominal of 18 µm only by 1.5%. The dispersion is most likely due to the rather thick photoresist mask required for selective protection of the topmost layer of SOI substrate in the Bosch process. Specific attention is paid to the exposure parameters to ensure verticality of generatrices in the lattice of openings. The achieved tilt angle is 88–89°. The lattice constants along with the contours of MMIPCs and PCWG integrated with HEB-loaded TSL are almost identical to those defined by EM model of the mixer. We also observe no notable distortion of the developed geometry of DRA arrays upon fabrication.

Our findings confirm robustness of the developed fabrication process. Thus, we plan to fabricate a series of THz HEB mixers with the proposed design to conduct detailed performance tests in the near future.

4. Conclusions

We propose the design of a SOI-based HEB mixer that utilizes photonic crystal waveguide integrated with two dielectric rod antenna arrays through multimode interference power combiners. This is to couple the mixer with a local oscillator and signal at 2.7 THz. The design is evaluated by both EM simulations and prototyping of the mixer key elements in a 50:1 scale. The developed on-chip power distribution networks ensure input losses of 2.4 dB and far-field radiation patterns with gain of 12.1 dB and a side lobe level below −11 dB. A full-sized prototype of the mixer designed for operation at 2.7 THz is successfully fabricated. The mixer is scalable to even higher operating frequencies in the range of 7–14 THz within the developed fabrication technology. Design tuning and detailed performance tests are in our future plans.

Author Contributions: Conceptualization, A.S.; methodology, A.S. and I.B.; software, A.S. and A.P.; validation, A.S. and I.B.; formal analysis, A.S., I.B. and A.P.; investigation, A.S., I.B., A.P. and M.E.; resources, I.B. and A.P.; data curation, A.S.; writing—original draft preparation, A.S.; writing—review and editing, A.S., I.B. and A.P.; visualization, A.S. and G.G.; supervision, G.G.; project administration, A.S.; funding acquisition, A.S. All authors have read and agreed to the published version of the manuscript.

Funding: This research was funded by the Russian Science Foundation, grant number 22-79-10279, https://rscf.ru/project/22-79-10279/ (accessed on 3 May 2023).

Institutional Review Board Statement: Not applicable.

Informed Consent Statement: Not applicable.

Data Availability Statement: Data are available upon reasonable request.

Acknowledgments: The authors would like to express their gratitude to Philipp Zolotov for their kind support in fabrication of superconducting structures.

Conflicts of Interest: The authors declare no conflict of interest.

Abbreviations

The following abbreviations are used in this manuscript:

THz	Terahertz
PIC	Photonic integrated circuit
PPDN	Photonic power distribution network
HEB	Hot electron bolometer
DRA	Dielectric rod antenna
LO	Local oscillator
SIS	Superconductor-insulator-superconductor
ISM	Interstellar medium
EM	Electromagnetic
MMIPC	Multimode interference power combiner
PCWG	Photonic crystal waveguide
TSL	Tapered slot line
3d	Three-dimensional
AC	Alternating current
IR	Infrared
DBR	Distributed Bragg reflector
CW	Continuous waveform
AM	Amplitude modulation
SOI	Silicon-on-insulator

References

1. Yu, L.; Hao, L.; Meiqiong, T.; Jiaoqi, H.; Wei, L.; Jinying, D.; Xueping, C.; Weiling, F.; Yang, Z. The medical application of terahertz technology in non-invasive detection of cells and tissues: Opportunities and challenges. *RSC Adv.* **2019**, *9*, 9354–9363. [CrossRef] [PubMed]
2. AlNabooda, M.O.; Shubair, R.M.; Rishani, N.R.; Aldabbagh, G. Terahertz spectroscopy and imaging for the detection and identification of illicit drugs. In Proceedings of the 2017 Sensors Networks Smart and Emerging Technologies (SENSET), Beirut, Lebanon, 12–14 September 2017; pp. 1–4.

3. Ma, Y.; Li, J.; Han, Z.; Maeda, H.; Ma, Y. Bragg-mirror-assisted high-contrast plasmonic interferometers: Concept and potential in terahertz sensing. *Nanomaterials* **2020**, *10*, 1385. [CrossRef] [PubMed]
4. Yang, K.; Li, J.; de la Chapelle, M.L.; Huang, G.; Wang, Y.; Zhang, J.; Xu, D.; Yao, J.; Yang, X.; Fu, W. A terahertz metamaterial biosensor for sensitive detection of microRNAs based on gold-nanoparticles and strand displacement amplification. *Biosens. Bioelectron.* **2021**, *175*, 112874. [CrossRef] [PubMed]
5. Withayachumnankul, W.; Fujita, M.; Nagatsuma, T. Integrated silicon photonic crystals toward terahertz communications. *Adv. Opt. Mater.* **2018**, *6*, 1800401. [CrossRef]
6. Kumar, A.; Gupta, M.; Pitchappa, P.; Wang, N.; Fujita, M.; Singh, R. Terahertz topological photonic integrated circuits for 6G and beyond: A Perspective. *J. Appl. Phys.* **2022**, *132*, 140901. [CrossRef]
7. Jha, K.R.; Singh, G. Analysis of narrow terahertz microstrip transmission-line on multilayered substrate. *J. Comput. Electron.* **2011**, *10*, 186–194. [CrossRef]
8. Cao, L.; Grimault-Jacquin, A.S.; Aniel, F. Comparison and optimization of dispersion, and losses of planar waveguides on benzocyclobutene (BCB) at THz frequencies: Coplanar waveguide (CPW), microstrip, stripline and slotline. *Prog. Electromagn. Res. B* **2013**, *56*, 161–183. [CrossRef]
9. Koala, R.A.; Fujita, M.; Nagatsuma, T. Nanophotonics-inspired all-silicon waveguide platforms for terahertz integrated systems. *Nanophotonics* **2022**, *11*, 1741–1759. [CrossRef]
10. Sengupta, K.; Nagatsuma, T.; Mittleman, D.M. Terahertz integrated electronic and hybrid electronic–photonic systems. *Nat. Electron.* **2018**, *1*, 622–635. [CrossRef]
11. Martini, F.; Cibella, S.; Gaggero, A.; Mattioli, F.; Leoni, R. Waveguide integrated hot electron bolometer for classical and quantum photonics. *Opt. Express* **2021**, *29*, 7956–7965. [CrossRef]
12. Karpov, A.; Miller, D.; Rice, F.; Stern, J.; Bumble, B.; LeDuc, H.; Zmuidzinas, J. Low Noise 1 THz–1.4 THz Mixers Using Nb/Al-AlN/NbTiN SIS Junctions. *IEEE Trans. Appl. Supercond.* **2007**, *17*, 343–346. [CrossRef]
13. Mehdi, I.; Siles, J.V.; Lee, C.; Schlecht, E. THz diode technology: Status, prospects, and applications. *Proc. IEEE* **2017**, *105*, 990–1007. [CrossRef]
14. Shurakov, A.; Lobanov, Y.; Goltsman, G. Superconducting hot-electron bolometer: From the discovery of hot-electron phenomena to practical applications. *Supercond. Sci. Technol.* **2015**, *29*, 023001. [CrossRef]
15. Stacey, G.J. THz low resolution spectroscopy for astronomy. *IEEE Trans. Terahertz Sci. Technol.* **2011**, *1*, 241–255. [CrossRef]
16. Silva, J.; Mirzaei, B.; Laauwen, W.; More, N.; Young, A.; Kulesa, C.; Walker, C.; Khalatpour, A.; Hu, Q.; Groppi, C.; et al. 4 × 2 HEB receiver at 4.7 THz for GUSTO. In *Millimeter, Submillimeter, and Far-Infrared Detectors and Instrumentation for Astronomy IX*; SPIE: Austin, TX, USA , 2018; Volume 10708, pp. 94–103.
17. Wiedner, M.C.; Mehdi, I.; Baryshev, A.; Belitsky, V.; Desmaris, V.; DiGiorgio, A.M.; Gallego, J.D.; Gerin, M.; Goldsmith, P.; Helmich, F.; et al. A proposed heterodyne receiver for the origins space telescope. *IEEE Trans. Terahertz Sci. Technol.* **2018**, *8*, 558–571. [CrossRef]
18. Shi, S.C.; Paine, S.; Yao, Q.J.; Lin, Z.H.; Li, X.X.; Duan, W.Y.; Matsuo, H.; Zhang, Q.; Yang, J.; Ashley, M.; et al. Terahertz and far-infrared windows opened at Dome A in Antarctica. *Nat. Astron.* **2016**, *1*, 0001. [CrossRef]
19. Balanis, C.A. *Antenna Theory: Analysis and Design*; John Wiley & Sons: Hoboken, NJ, USA, 1997.
20. Cheng, L.; Mao, S.; Li, Z.; Han, Y.; Fu, H. Grating couplers on silicon photonics: Design principles, emerging trends and practical issues. *Micromachines* **2020**, *11*, 666. [CrossRef]
21. Bakke, T.; Sullivan, C.T.; Mukherjee, S.D. Polymeric optical spot-size transformer with vertical and lateral tapers. *J. Light. Technol.* **2002**, *20*, 1188. [CrossRef]
22. James, J.R. Engineering approach to the design of tapered dielectric-rod and horn antennas. *Radio Electron. Eng.* **1972**, *42*, 251–259. [CrossRef]
23. Shiau, Y. Dielectric rod antennas for millimeter-wave integrated circuits (short papers). *IEEE Trans. Microw. Theory Tech.* **1976**, *24*, 869–872. [CrossRef]
24. Lobanov, Y.; Shcherbatenko, M.; Shurakov, A.; Rodin, A.V.; Klimchuk, A.; Nadezhdinsky, A.I.; Maslennikov, S.; Larionov, P.; Finkel, M.; Semenov, A.; et al. Heterodyne detection at near-infrared wavelengths with a superconducting NbN hot-electron bolometer mixer. *Opt. Lett* **2014**, *39*, 1429–1432. [CrossRef] [PubMed]
25. Chau, Y.F.; Yang, T.J.; Lee, W.D. Coupling technique for efficient interfacing between silica waveguides and planar photonic crystal circuits. *Appl. Opt.* **2004**, *43*, 6656–6663. [CrossRef] [PubMed]
26. Soldano, L.B.; Pennings, E.C. Optical multi-mode interference devices based on self-imaging: Principles and applications. *J. Light. Technol.* **1995**, *13*, 615–627. [CrossRef]
27. Tesmer, H.; Reese, R.; Polat, E.; Nickel, M.; Jakoby, R.; Maune, H. Fully dielectric rod antenna arrays with integrated power divider. *Frequenz* **2019**, *73*, 367–377. [CrossRef]
28. Prikhodko, A.; Belikov, I.; Lvov, A.; Shurakov, A.; Goltsman, G. Millimeter wave photonic crystal waveguides fabricated via direct machining. *St. Petersburg State Polytech. Univ. J. Phys. Math.* **2022**, *15*, 345–349.